doi:10.1088/1742-6596/2767/5/052005

Data-driven met-ocean model for offshore wind energy applications

Kianoosh Yousefi^{1, 2}, Gurpreet S. Hora³, Hongshuo Yang⁴, and Marco Giometto³

- ¹ Department of Mechanical Engineering, University of Texas at Dallas, Richardson, TX, USA
- ² Center for Wind Energy, University of Texas at Dallas, Richardson, TX, USA
- ³ Department of Civil Engineering and Engineering Mechanics, Columbia University, New York, NY, USA
- ⁴ Department of Computer Science, Columbia University, New York, NY, USA

E-mail: kyousefi@utdallas.edu E-mail: gh2546@columbia.edu

Abstract. In recent years, the global transition towards green energy, driven by environmental concerns and increasing electricity demands, has remarkably reshaped the energy landscape. The transformative potential of marine wind energy is particularly critical in securing a sustainable energy future. To achieve this objective, it is essential to have an accurate understanding of wind dynamics and their interactions with ocean waves for the proper design and operation of offshore wind turbines (OWTs). The accuracy of met-ocean models depends critically on their ability to correctly capture sea-surface drag over the multiscale ocean surface—a quantity typically not directly resolved in numerical models and challenging to acquire using either field or laboratory measurements. Although skin friction drag contributes considerably to the total wind stress, especially at moderate wind speeds, it is notoriously challenging to predict using physics-based approaches. The current work introduces a novel approach based on a convolutional neural network (CNN) model to predict the spatial distributions of skin friction drag over wind-generated surface waves using wave profiles, local wave slopes, local wave phases, and the scaled wind speed. The CNN model is trained using a set of high-resolution laboratory measurements of air-side velocity fields and their respective surface viscous stresses obtained over a range of wind-wave conditions. The results demonstrate the capability of our model to accurately estimate both the instantaneous and area-aggregate viscous stresses for unseen wind-wave regimes. The proposed CNN-based wall-layer model offers a viable pathway for estimating the local and averaged skin friction drag in met-ocean simulations.

1. Introduction

The global shift towards clean energy resources, driven by both environmental concerns and increasing electricity demands, has reshaped the energy landscape. The transformative potential of marine wind energy is critical for achieving the global clean energy goals. In the case of US only, the current 30 MW installed offshore wind energy capacity of the US is projected to increase to 30 GW by 2030, setting the nation on a pathway to 110 GW by 2050 [1–3]. This exponential growth underscores the integral role of offshore wind energy in the energy matrix, reflecting its potential and the increasing reliance on sustainable sources. Despite the advantages of offshore wind turbines (OWTs) due to stronger and stable wind speed conditions, locations away from populated areas, and more open space available [4–6], they are subjected to a harsh environment characterized by constant interactions with both wind and wave forces [7–9]. Hence, an accurate understanding and characterization of wind dynamics and their interplay with ocean waves is essential to properly design and operate large offshore wind farms. In particular, advances in coupled high-resolution meteorological and oceanographic (met-ocean) models offer a fruitful pathway to achieve this objective.

Content from this work may be used under the terms of the Creative Commons Attribution 4.0 licence. Any further distribution of this work must maintain attribution to the author(s) and the title of the work, journal citation and DOI.

doi:10.1088/1742-6596/2767/5/052005

Although field measurements have delved into the dynamics of turbine wakes in offshore farms [10–12], they fall short of elucidating the influence of ocean waves on wake structures and wind-wave-wake interactions. Laboratory efforts, like those by Ferčák et al. [13] and Bossuyt et al. [14], have attempted to bridge this gap, but inherent limitations prevent them from replicating the full range of offshore conditions. In addition, due to the many scales present at the sea surface, high-fidelity numerical simulations are equally challenging and have severe limitations. In particular, large-eddy simulations (LESs) have been shown to yield high-fidelity results for flow over the complex sea surface by resolving the large- and intermediate-scale turbulent motions [15–19]. In recent years, computational studies [20–23] have provided a better understanding of wind and wave interactions and their impact on offshore wind farm dynamics and performance. However, resolving the near-surface turbulent flow structures demands a high computational resolution, which becomes prohibitively costly under a realistic range of diverse sea states and offshore turbulence parameters. As a result, the near-surface region is typically bypassed through a so-called wall-layer model [24,25] that directly resolves only a portion of the surface drag variability and models the unresolved drag contributions.

For atmospheric boundary-layer flows, it is customary to rely on simple, bulk wall-layer models based on the Monin-Obukhov similarity theory (MOST) [17, 26]. However, MOST-based parametrizations are only valid under equilibrium conditions and lack sea state awareness. In general, the drag at the ocean surface strongly depends on environmental conditions and is a function of not only wind speed but also wave height, wave slope, wind-wave alignment, and wave age. As such, these models often struggle to accurately predict the evolution of wave fields [27–32]. Further, while more advanced models do exist to predict pressure-drag contributions for wind-wave boundary layers [33–35], no model yet is able to accurately capture skin friction contributions. For example, Aiyer et al. [35] recently developed a sea-surface form drag model (based on the surface gradient drag model of Anderson & Meneveau [36]) for LES of wind-wave interactions that can estimate the air-sea momentum flux without the need for a separate solver for the wavefield. However, although skin friction contributions may be small in high wind conditions, they represent a significant percentage of the total wind stress at low-moderate wind speeds (i.e., wind speeds smaller than approximately 10 m/s) [37-39]. For example, at low wind speeds of about 2 m/s, the surface tangential stress accounts for more than 80% of the total stress at the air-water interface, and it remains significant by contributing more than 35% to the wind stress even for wind speeds of approximately 10 m/s [37-39]. Thus, their accurate representations in met-ocean models are crucial for OWTs design, given that the average wind speed at the hub height is typically at moderate wind speeds.

The accurate prediction of wind-wave interactions hinges upon the model's ability to capture sea-surface drag over multiscale ocean surfaces—a notoriously challenging task due to the presence of complex interfacial mechanisms. In the absence of accurate physics-based sea-surface drag models [40,41], machine learning (ML) approaches may offer a practical alternative. Nonetheless, despite various applications of ML methods in the field of fluid mechanics and turbulence research [42–45], their utilization in air-sea interaction studies has been predominantly focused on estimating statistical wave characteristics such as significant wave height and peak wave period [46–51]. Yet, the feasibility of using ML techniques to reconstruct the turbulent flow over/below surface waves requires to be explored in more detail. In the present study, we employ a convolutional neural network (CNN) model to predict the skin friction drag solely from wave profiles and the scaled wind speed. The developed CNN model inputs surface wave profiles and 10 m wind speed scaled with wave phase celerity and predicts skin friction drag distributions over wind-driven waves. The CNN is trained using laboratory measurements of velocity fields obtained over a range of wind-wave conditions. Our model accurately predicts instantaneous and area-aggregate viscous stresses for unseen wind waves, thus contributing to addressing an important knowledge gap in met-ocean simulations. The proposed CNN model can be easily tailored to serve as a wall-layer model for skin friction contributions in wall-modeled LESs of airflow over wave fields. We particularly showed that the proposed ML-based model could accurately estimate both instantaneous and averaged viscous stresses for unseen wind-driven waves within the training dataset using surface signatures and wave age information only.

doi:10.1088/1742-6596/2767/5/052005

The rest of the paper is organized as follows. The methodology, including theoretical background and experimental data description, is provided in Section 2. Section 3 details the ML-based modeling approach. The results are presented in Section 4, in which we have assessed the performance of the CNN model and discuss its capability in reconstructing skin friction drag. The application of the model to met-ocean modeling and offshore wind energy is briefly explained in Section 5. Finally, a brief conclusion is presented in Section 6.

2. Methodology

2.1. Theoretical Background

The action of wind induces both momentum and energy fluxes to the ocean surface. The total momentum flux at the air-water interface, or equivalently wind stress, is the sum of skin friction and form drag, i.e.,

$$\tau = \tau_{\nu} + \tau_{f},\tag{1}$$

where τ_{ν} is the local interfacial shear stress (i.e., skin friction drag) and τ_f is the form drag induced by pressure forces. By definition, the surface shear stress is the tangent component of the stress tensor, acting parallel to the surface. It can then be obtained by

$$\tau_{\mathcal{V}} = (\boldsymbol{\tau}\boldsymbol{n}) \cdot \boldsymbol{t},\tag{2}$$

where $\tau = \mu \left(\nabla u + \nabla u^T \right)$ is the airside stress tensor, μ is the absolute viscosity, ∇u is the velocity gradient tensor, ∇u^T is the transpose of the velocity gradient tensor, u = (u, w) is the velocity vector, and (n, t) are local normal and tangent unit vectors. Given the two-dimensional velocity field with a streamwise velocity component in the direction of wave propagation, the skin friction drag can then be estimated by

$$\tau_{\nu} = \mu \left(\frac{\partial u}{\partial z} + \frac{\partial w}{\partial x} \right) + 2\mu \frac{\partial \eta}{\partial x} \left(\frac{\partial w}{\partial z} - \frac{\partial u}{\partial x} \right), \tag{3}$$

where (u, w) are streamwise and vertical velocities, (x, z) are streamwise and vertical coordinates, $\partial \eta / \partial x \equiv \varepsilon$ represents the local wave slope, and η is the surface elevation. Here, the skin friction drag is estimated to the first order in wave slope [39,52]. The form drag can also be expressed by

$$\tau_f = p_s \frac{\partial \eta}{\partial x},\tag{4}$$

where p_s is pressure at the interface. However, we only focus on the skin friction drag. For a comprehensive understanding of sea-surface form drag, we refer the reader to the relevant literature (e.g., [17, 19, 53–58]).

2.2. Experimental Dataset

To train and examine the CNN model, we used the existing raw dataset of Yousefi et al. [37,59]. The dataset set consists of high-resolution velocity measurements above surface waves, acquired using particle image velocimetry (PIV) and laser-induced fluorescence (LIF) techniques in the wind-wave tunnel facility of the University of Delaware. The wave tank of the facility is approximately 42 m long, 1 m wide, and 1.25 m high, of which only 0.7 m filled with fresh water to ensure sufficient airflow space above the air-water interface. The LIF technique was employed in combination with PIV to precisely detect surface profiles within the PIV field of view. This allowed the acquisition of velocity measurements close to the surface within the airside viscous sublayer, at about 100 µm above the surface. Experimental measurements were performed for various wind-wave cases with 10-m equivalent wind speeds of 5.08, 9.57, and 14.82 m/s (moderate-strong wind speeds). It should be noted here that we only considered wind-driven surface waves [40] under no current. In addition, the wind and wave propagation directions were aligned in the streamwise direction. The experimental conditions are listed in Table 1. The facility, experimental setup, and image acquisition and processing procedures are described at length in [60].

doi:10.1088/1742-6596/2767/5/052005

Table 1. Summary of the experimental data and CNN performance in predicting skin friction drag. The apparent peak wave frequency (denoted by f) and wave celerity (denoted by C) were obtained from wave height signals. The friction and 10-m velocities were calculated from the mean velocity profiles.

	U_{10} (m s ⁻¹)	u_* (m s ⁻¹)	C/U_{10}	C/u_*	λ (m)	ak	f (Hz)	RMAE	\mathbb{R}^2
E-W05	5.08	0.168	0.12	3.69	0.25	0.13	2.5	0.26	0.91
E-W09	9.57	0.318	0.08	2.46	0.39	0.19	2.0	0.25	0.91
E-W14	14.82	0.567	0.06	1.53	0.48	0.26	1.8	0.29	0.88

Examples of streamwise velocity measurements, along with the corresponding skin friction drag (calculated as explained above), are shown in Fig. 1 over non-separating and separating wind waves with a wind speed of $U_{10} = 5.08$ m/s. Here, the velocity fields are normalized by 10-m wind velocity and the surface shear stress is scaled by the total stress, $\tau = \rho u_*^2$. Over the separating wind wave, while the skin friction reaches its peak value upstream of the wave crest, it significantly drops downstream due to airflow separation. In fact, the skin friction becomes negative on the leeward side and remains approximately zero within the separation bubble. The surface viscous stress gradually recovers past the separated region and increases to a positive value. In contrast, over the non-separating wind wave, the surface viscous stress remains positive across the entire wave profile and contributes significantly to the total wind stress. The experimental dataset consists of approximately 11,300 PIV images, which were split into 80% training, 10% validation, and 10% test sub-datasets.

3. Machine Learning Model

This study aims to develop a data-driven model to accurately estimate the spatial distribution of skin friction drag of surface wind waves from wave profiles, local slope, local wave phases, and the wind speed scaled by the wave celerity. In particular, we aim to develop a mapping such that

$$\mathcal{M}: (C/U_{10}, \eta, \varepsilon, \varphi) \to \tau_{\nu},$$
 (5)

in which C is the wave celerity defined as the phase speed of the peak energy in the wave-height spectrum,

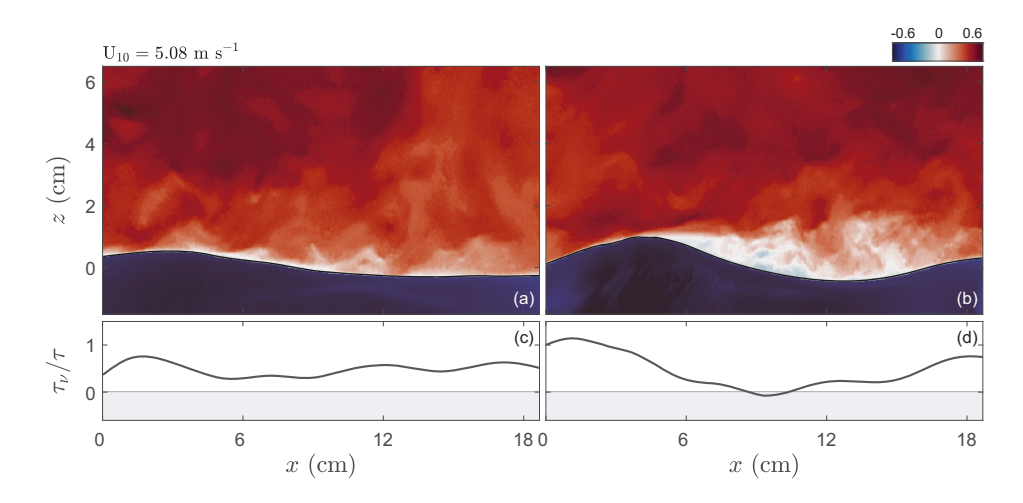


Figure 1. An example of the experimental data. The instantaneous streamwise velocities are shown on top panels along with the corresponding skin friction over a non-separating (left-hand column) and separating (right-hand column) wind wave for the wind-wave condition of $U_{10} = 5.08$ m/s.

doi:10.1088/1742-6596/2767/5/052005

 U_{10} is the wind speed at the reference height of 10 m above the ocean surface, and φ is the local wave phases. The ratio C/U_{10} is called the wave age in the wind-wave-current literature, serving as a surrogate variable for different sea states. To approximate the above mapping, we employ a CNN-based ML model. This choice is well-motivated due to the CNN model's distinguished performance in non-linear multi-output regression tasks involving structured grid data, such as velocity fields, across a wide spectrum of scientific and engineering problems [61–64]. These models excel at capturing spatially local features through filter-based convolutions, exhibit translation equivariance crucial for many physical problems, and offer scalability advantages [61,65].

The CNN model is thus tailored in such a way that

$$\tau_{\nu} \approx f(C/U_{10}, \, \eta, \, \varepsilon, \, \varphi; \, \theta),$$
(6)

where θ represents the parameters of the CNN model that are learned during the training process. To determine the optimal parameters θ of the mapping function, we employ the mean squared error (MSE) loss augmented with ridge regularization (also referred to as L₂ regularization). This technique serves as a preventive measure against overfitting by incorporating a penalty term into the loss function. This penalty term is proportional to the squared magnitudes of the model's trainable parameters (i.e., θ_j), thus encouraging smaller weights and reducing the complexity of the model, and enhancing generalization performance [61,66]. In essence, the goal is to minimize the following objective function:

$$\theta = \arg\min_{\theta} \left[\frac{1}{N} \sum_{i=1}^{N} (\hat{\tau}_{\nu,i} - \tau_{\nu,i})^2 \right] + \lambda \sum_{i=1}^{K} \theta_j^2 , \qquad (7)$$

where $\hat{\tau}_{\nu}$ and τ_{ν} represent the CNN model prediction and its corresponding ground truth experimental result, λ is the regularization parameter, N is the number of training samples, and K is the number of trainable parameters. This optimization process enables the CNN model to learn optimal parameters, improving its ability to approximate the underlying mapping function.

The CNN model is implemented using the Pytorch library. The f architecture comprises five convolutional layers, one flatten layer, and two dense layers with Mish nonlinearity [67], defined as $Mish(x) = x \tanh[\log(1+e^x)]$, applied to all layers except the output layer (which remains linear). For all convolutional layers, the filter size and number of kernels are set to 3 and 8, respectively. The non-linear dense layer contains 2,000 perceptrons, while the output layer contains 985 perceptrons. The optimal CNN-based ML model architecture is illustrated in Figure 2, which has 65,015,401 trainable parameters (weights and biases) and 0 non-trainable parameters. The architectural details of the CNN model, including the feature shapes, nonlinearity functions, and the number of trainable parameters associated with each layer, are also provided in Table 2 for completeness. The trainable parameters are initialized randomly using values sampled from a uniform distribution, as suggested in [68]. The value of regularization parameter λ is set to 10^{-4} and it is trained end-to-end using backpropagation with the Adam optimizer [69]. We employ a reduced learning rate on a plateau schedule, starting at 5×10^{-4} and reducing it by a factor of 0.9 when the validation loss plateaus during training. The effective mini-batch size during the training phase is set to 64.

Here, it should be noted that the CNN model has been trained over an experimental dataset that only consists of wind-generated surface waves. The wave age of surface waves covers a small range of wind waves in these constant fetch laboratory experiments. This resulted in waves that only propagate in the streamwise direction such that wave groups and individual waves within those groups generally align in the same direction. Therefore, the proposed model may not be applicable for complex seas with the presence of swell and the resulting wind-wave misalignment in the wavefield. In addition, the complications of breaking waves and the generation of bubbles and/or spray were largely avoided in these experimental conditions. As such, the model may not be valid for wavefields with frequent breaking events. Finally, the model lacks temporal awareness, and the mapping does not account for memory effects and historical events (for details, see [70–73]).

doi:10.1088/1742-6596/2767/5/052005

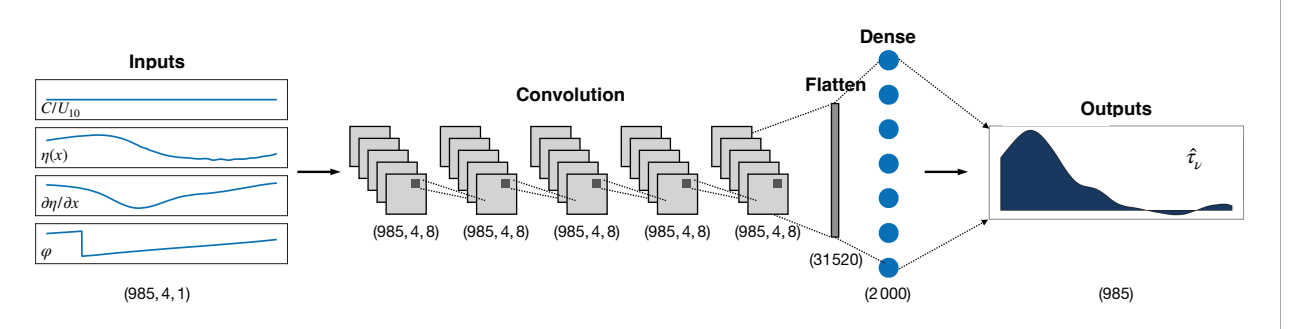


Figure 2. Schematic of the CNN architecture used for estimating the skin friction drag, τ_{ν} , from wave profiles, η , local wave slopes, $\partial \eta/\partial x$, wave phases, φ , and wave age, C/U_{10} . The architecture comprises five convolution layers, one flatten layer, and two dense layers with Mish nonlinearity applied to all except the output dense layer. Each convolutional layer employs a filter size of three with eight filters. The non-linear dense layer comprises 2,000 perceptrons, while the output dense layer contains 985 perceptrons.

4. Results and Discussion

In order to assess the performance of the CNN model in reconstructing skin friction drag, we first inspect the along-wave distributions of surface viscous stress and the model's ability to capture the effects of near-surface separation on the skin friction drag (as described in the previous section). Figure 3 shows the predicted instantaneous skin friction drag scaled with total stress ($\hat{\tau}_{\nu}/\tau$) for cases with a wind speed of 5.08, 9.57, and 14.82 m/s along with their respective experimental data for comparison. For reference, the instantaneous streamwise velocity fields are also shown on top the panels. The CNN model successfully reconstructed the spatial distribution of the tangential stress, with minor discrepancies in the peak magnitudes. The model is particularly effective in predicting airflow separation regions downstream of waves.

To quantify the performance of the model, we computed the coefficient of determination (R^2) on the test dataset (reported in Table 1). The R^2 is roughly 0.91, 0.91, and 0.88 for wind-wave cases with $U_{10} = 5.08$, 9.57, and 14.82 m/s, respectively, highlighting a high accuracy. Model performance slightly declines with increasing wind speed, in part due to limitations of PIV measurements in capturing full wave profiles and increased signal-to-noise ratio at higher wind speeds. These findings highlight the ML model's good performance when at least one wavelength is adequately captured in the experimental field of view.

The wave-phase-averaged predictions of the scaled skin friction drag, $\langle \hat{\tau}_{\nu} \rangle / \tau$, are also shown and compared with corresponding measurements in Fig. 4 for a wind speed of 5.08 m/s. The phase-averaging procedure is described in more detail in [37]. Briefly, the phase-averaged stress data are bin averaged

Table 2. Architectural specifications of the CNN model designed for predicting skin friction drag, τ_{ν} . Here, Conv indicates the convolutional layer and Dense 2 represents the output layer.

Layer	Shape	Non linearity	Number of Parameters	
Input	(985,4,1)	_	_	
Conv 1	(985,4,8)	Mish	80	
Conv 2	(985,4,8)	Mish	584	
Conv 3	(985,4,8)	Mish	584	
Conv 4	(985,4,8)	Mish	584	
Conv 5	(985,4,8)	Mish	584	
Flatten	(31520)	_	_	
Dense 1	(2000)	Mish	63,0420,00	
Dense 2	(985)	Linear	19,709,85	

doi:10.1088/1742-6596/2767/5/052005

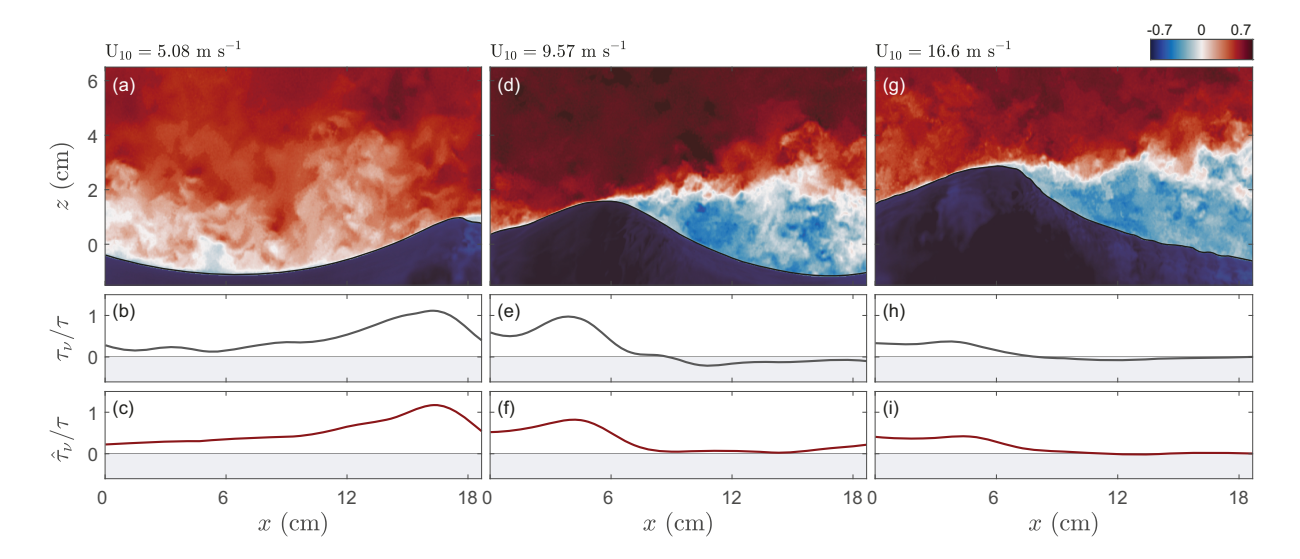


Figure 3. Spatial distributions of normalized skin friction drag obtained from experiments (b, e, h) and reconstructed by the CNN model (c, f, i) for wind-wave conditions of E-W05 (left-hand column), E-W09 (middle column), and E-W14 (right-hand column). Also, for reference, normalized instantaneous streamwise velocity fields (u/U_{10}) are plotted on top panels.

according to the local phase of the surface wave profile. In a wave-phase-averaged sense, the CNN prediction of surface shear stress particularly shows an excellent agreement with the experiment, where it presents an along-wave asymmetry pattern in which the stress is highest upwind of the wave crest and a minimum in the middle of the leeward side. The same order of accuracy was also observed for other experimental cases (not shown here for brevity). Further, to examine the proposed model in reconstructing the spatial variability of phase-averaged skin friction drag, the pdf of $\langle \tau_{\nu} \rangle / \tau$ for both CNN predictions and measurements is depicted in Fig. 4(c). The pdf plots of the reconstructed viscous stress align remarkably with those derived from the experiments. These findings underscore the model's proficiency in predicting the spatial distribution of phase-averaged skin friction drag.

5. Application to Wind Energy

In the context of offshore wind energy, predicting surface drag, both in terms of its area-aggregate and spatial distribution, holds scientific significance for several key reasons. Firstly, surface drag modeling is pivotal for calculating the available wind energy that wind turbines can extract efficiently. Secondly, surface drag helps in understanding and optimizing the development and propagation of wakes generated by wind turbines. This knowledge aids in designing wind farms with improved turbine spacing and layout for maximum energy production. Similarly, surface drag variability introduces uncertainty into wind energy assessments, which can affect investment and project financing decisions. Reducing this uncertainty is essential for project viability. Furthermore, precise estimates of surface drag variability enable the assessment and mitigation of the effects of extreme winds and turbulence on wind turbine performance and reliability. Lastly, accurate knowledge of surface drag is necessary for evaluating the environmental impact of offshore wind farms, including factors like sediment transport and water column mixing, which can affect marine ecosystems and habitats. As mentioned in the preceding sections, the proposed model can be readily incorporated in LES as a wall-layer model for skin friction, thus providing a useful tool for optimizing OWT energy extraction while ensuring turbine reliability and mitigating negative environmental impacts.

doi:10.1088/1742-6596/2767/5/052005

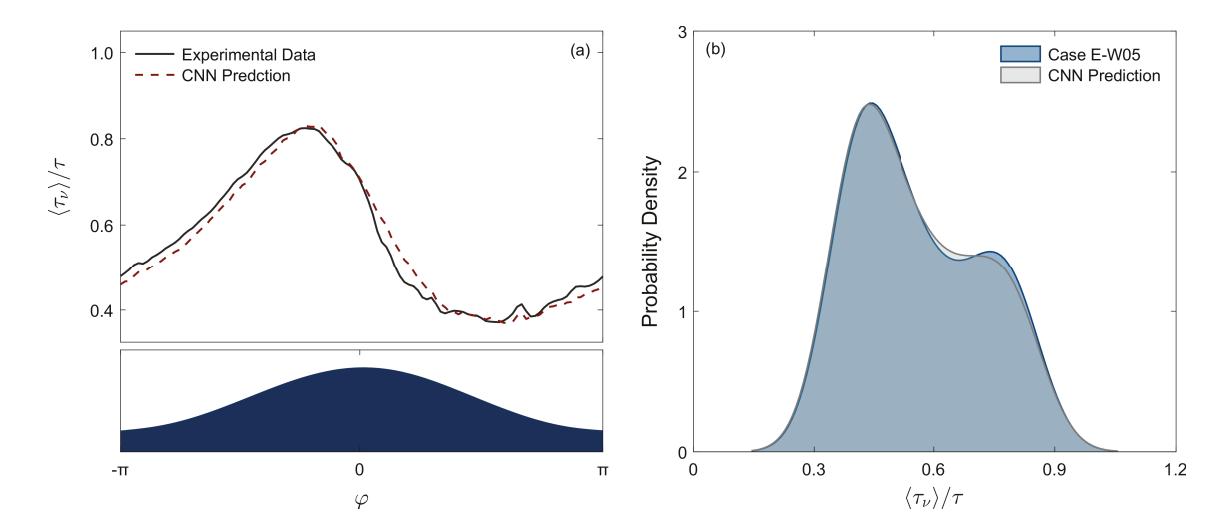


Figure 4. (a) CNN prediction of the phase-averaged skin friction drag, $\langle \tau_{\nu} \rangle / \tau$, compared to the experimental measurements for the case with a wind speed of 5.08 m/s. All stress profiles are scaled using the total wind stress. In panel (b), the probability density function of $\langle \tau_{\nu} \rangle / \tau$ estimated by CNN model and experimental measurements is plotted for the same wind-wave case.

6. Summary

In this work, we investigated the performance of a CNN model in predicting the skin friction drag of surface wind waves using wave profiles and wave age. The model utilized a combination of convolutional, dense, and Mish non-linear layers to extract information from a two-dimensional discrete grid of wave variables, including the wave profile, local wave slope, wave phases, wave age, and surface viscous stress. The model was trained and evaluated using high-resolution velocity measurements over a range of wind-wave conditions with wind speeds of 5.08–14.82 m/s. Overall, the model demonstrated excellent performance in accurately reconstructing skin friction drag. This was verified through an error analysis using relative mean and coefficient of determination error metrics and a qualitative inspection of instantaneous stress profiles. However, despite the model's effectiveness, we observed a slight increase in the error metrics with increasing wind speed. Moreover, considering the wave phase dependency, the distribution of skin friction drag over surface waves is investigated, as this factor is relevant to numerical models. The CNN model exhibited optimal performance near the wave crest, while its accuracy slightly decreased on the leeward side of the waves, where airflow separation events occur. This study demonstrates that the CNN-based model is a promising technique for effectively reconstructing skin friction drag. Importantly, to the author's knowledge, it marks the first successful attempt in the literature to model sea-surface drag solely based on surface signatures. The ability to accurately predict the spatial distribution of skin friction over surface waves has significant implications from a wind energy perspective.

Acknowledgments

This research was partly supported by the National Science Foundation (NSF) through grant numbers CCF-2030859 (to the CRA for the Computing Innovation Fellows Project) and CBET-2404368. The presenting author is also grateful to the Center for Wind Energy at the University of Texas at Dallas for providing support for conference registration and travel. KY and GSH contributed equally to this work.

References

- [1] Musial W D, Beiter P C, Spitsen P, Nunemaker J and Gevorgian V 2019 2018 offshore wind technologies market report Tech. rep. National Renewable Energy Lab.(NREL), Golden, CO (United States)
- [2] Lee J and Zhao F 2021 Global Wind Energy Council 75
- [3] Bugnot A, Mayer-Pinto M, Airoldi L, Heery E, Johnston E, Critchley L et al. 2021 Nature Sustainability 4 33-41

doi:10.1088/1742-6596/2767/5/052005

- [4] Esteban M D, Diez J J, López J S and Negro V 2011 Renewable energy 36 444-450
- [5] Castro-Santos L, Martins E and Soares C G 2017 Energy 140 1121-1130
- [6] Rusu E and Onea F 2018 Clean Energy 2 10-19
- [7] Paulsen B T, de Sonneville B, van der Meulen M and Jacobsen N G 2019 Coastal Engineering 143 76-95
- [8] Lin Y H and Hasan A D 2022 Journal of Renewable and Sustainable Energy 14
- [9] Zhu J, Gao Y, Wang L and Li W 2022 Marine Structures 86 103270
- [10] Christiansen M B and Hasager C B 2005 Remote Sensing of Environment 98 251-268
- [11] Barthelmie R J, Hansen K, Frandsen S T, Rathmann O, Schepers J, Schlez W, Phillips J, Rados K, Zervos A, Politis E et al. 2009 Wind Energy: An International Journal for Progress and Applications in Wind Power Conversion Technology 12 431–444
- [12] Platis A, Siedersleben S K, Bange J, Lampert A, Bärfuss K, Hankers R, Cañadillas B, Foreman R, Schulz-Stellenfleth J, Djath B et al. 2018 Scientific reports 8 2163
- [13] Ferčák O, Bossuyt J, Ali N and Cal R B 2022 Applied Energy 309 118358
- [14] Bossuyt J, Ferčák O, Sadek Z, Meneveau C, Gayme D F and Cal R B 2023 Physical Review Fluids 8 120501
- [15] Sullivan P P, Edson J B, Hristov T and McWilliams J C 2008 Journal of the Atmospheric Sciences 65 1225–1245 ISSN 0022-4928
- [16] Sullivan P P, McWilliams J C and Patton E G 2014 Journal of the Atmospheric Sciences 71 4001–4027 ISSN 0022-4928
- [17] Hara T and Sullivan P P 2015 Journal of Physical Oceanography 45 868–883 ISSN 0022-3670
- [18] Husain N, Hara T, Buckley M, Yousefi K, Veron F and Sullivan P 2019 Journal of Physical Oceanography 49 1997–2015
- [19] Hao X and Shen L 2019 Journal of Fluid Mechanics 874 391-425
- [20] Yang D, Meneveau C and Shen L 2014 Physics of Fluids 26
- [21] AlSam A, Szasz R and Revstedt J 2015 Journal of Energy Resources Technology 137 051209
- [22] Vollmer L, Steinfeld G and Kühn M 2017 Wind energy science 2 603-614
- [23] Yang H, Ge M, Abkar M and Yang X I 2022 Energy 256 124674
- [24] Piomelli U 2008 Progress in Aerospace Sciences 44 437-446
- [25] Bose S T and Park G I 2018 Annual Review of Fluid Mechanics 50 535-561
- [26] Hara T and Belcher S E 2004 Journal of Physical Oceanography 34 2345–2358 ISSN 0022-3670
- [27] Moon I J, Hara T, Ginis I, Belcher S E and Tolman H L 2004 Journal of the Atmospheric Sciences 61 2321-2333
- [28] Moon I J, Ginis I and Hara T 2004 Journal of the Atmospheric Sciences 61 2334-2348
- [29] Donelan M A, Curcic M, Chen S S and Magnusson A K 2012 Journal of Geophysical Research: Oceans 117
- [30] Cronin M F, Gentemann C L, Edson J, Ueki I, Bourassa M, Brown S, Clayson C A, Fairall C W, Farrar J T, Gille S T, Gulev S, Josey S A, Kato S, Katsumata M, Kent E, Krug M, Minnett P J, Parfitt R, Pinker R T, Stackhouse P W, Swart S, Tomita H, Vandemark D, Weller A R, Yoneyama K, Yu L and Zhang D 2019 Frontiers in Marine Science 6
- [31] Husain N T, Hara T and Sullivan P P 2022 Journal of Physical Oceanography 52 119-139
- [32] Husain N T, Hara T and Sullivan P P 2022 Journal of Physical Oceanography 52 141-159
- [33] Yang D, Meneveau C and Shen L 2013 Journal of Fluid Mechanics 726 62-99
- [34] Yang D, Shen L and Meneveau C 2013 Flow, Turbulence and Combustion 91 541-563
- [35] Aiyer A K, Deike L and Mueller M E 2023 Journal of the Atmospheric Sciences 80 49-62
- [36] Anderson W and Meneveau C 2010 Boundary-layer meteorology 137 397-415
- [37] Yousefi K, Veron F and Buckley M P 2020 Journal of Fluid Mechanics 895 A15 ISSN 0022-1120
- [38] Yousefi K, Veron F and Buckley M P 2020 Recent Advances in the Study of Oceanic Whitecaps ed Vlahos P and Monahan E C (Cham, Switzerland: Springer) chap 6, pp 77–94 ISBN 978-3-030-36371-0
- [39] Buckley M P, Veron F and Yousefi K 2020 Journal of Fluid Mechanics 905 A31 ISSN 0022-1120
- [40] Sullivan P P and McWilliams J C 2010 Annual Review of Fluid Mechanics 42 19-42 ISSN 0066-4189
- [41] Ayet A and Chapron B 2022 Boundary-Layer Meteorology 183 1–33
- [42] Kutz J N 2017 Journal of Fluid Mechanics 814 1-4
- [43] Brenner M, Eldredge J and Freund J 2019 Physical Review Fluids 4 100501
- [44] Brunton S L, Noack B R and Koumoutsakos P 2020 Annual Review of Fluid Mechanics 52 477-508
- [45] Fukami K, Fukagata K and Taira K 2020 Theoretical and Computational Fluid Dynamics 34 497–519
- [46] Rasp S and Lerch S 2018 Monthly Weather Review 146 3885-3900
- [47] James S C, Zhang Y and O'Donncha F 2018 Coastal Engineering 137 1-10
- [48] O'Donncha F, Zhang Y, Chen B and James S C 2018 Journal of Marine Systems 186 29–36
- [49] Zhang J, Zhao X, Jin S and Greaves D 2022 Applied Energy 324 119711
- [50] Dakar E, Fernández Jaramillo J M, Gertman I, Mayerle R and Goldman R 2023 Coastal Engineering Journal 1-16
- [51] Xu G, Zhang S and Shi W 2023 Ocean Engineering 267 113218
- [52] Longuet-Higgins M S 1969 Physics of Fluids 12 737–740
- [53] Banner M L 1990 Journal of Fluid Mechanics 211 463-495 ISSN 0022-1120
- [54] Sullivan P P, McWilliams J C and Moeng C H 2000 Journal of Fluid Mechanics 404 47-85 ISSN 00221120
- [55] Donelan M A, Babanin A V, Young I R and Banner M L 2006 Journal of physical oceanography 36 1672-1689

doi:10.1088/1742-6596/2767/5/052005

- [56] Peirson W L and Garcia A W 2008 Journal of Fluid Mechanics 608 243-274 ISSN 0022-1120
- [57] Yang D I and Shen L 2010 Journal of Fluid Mechanics 650 131–180 ISSN 0022-1120
- [58] Grare L, Lenain L and Melville W K 2013 Journal of Physical Oceanography 43 2156-2172 ISSN 0022-3670
- [59] Yousefi K, Veron F and Buckley M P 2021 Journal of Fluid Mechanics 920 A33
- [60] Yousefi K 2020 Turbulence in the atmospheric wave boundary layer (University of Delaware)
- [61] Goodfellow I, Bengio Y and Courville A 2016 Deep learning (MIT press)
- [62] Fukami K, Fukagata K and Taira K 2021 Journal of Fluid Mechanics 909 A9
- [63] Kim H, Kim J, Won S and Lee C 2021 Journal of Fluid Mechanics 910
- [64] Xuan A and Shen L 2023 Journal of Fluid Mechanics 959 A34
- [65] Gao H, Sun L and Wang J X 2021 Journal of Computational Physics 428 110079
- [66] Hastie T 2020 Technometrics 62 426-433
- [67] Misra D 2019 arXiv preprint arXiv:1908.08681
- [68] Glorot X and Bengio Y 2010 *Proceedings of the thirteenth international conference on artificial intelligence and statistics* (JMLR Workshop and Conference Proceedings) pp 249–256
- [69] Kingma D P and Ba J 2014 arXiv preprint arXiv:1412.6980
- [70] Hochreiter S and Schmidhuber J 1997 Neural computation 9 1735–1780
- [71] Vaswani A, Shazeer N, Parmar N, Uszkoreit J, Jones L, Gomez A N, Kaiser L and Polosukhin I 2017 Advances in Neural Information Processing Systems 30
- [72] Bai S, Kolter J Z and Koltun V 2018 arXiv preprint arXiv:1803.01271
- [73] Yousefi K, Hora G S, Yang H, Veron F and Giometto M G 2024 Journal of Fluid Mechanics 983 A9